HHS Public Access

Author manuscript

Opt Lett. Author manuscript; available in PMC 2017 January 02.

Published in final edited form as:

Opt Lett. 2013 July 01; 38(13): 2339–2341.

X-ray luminescence optical tomography imaging: experimental studies

Changqing Li[1,2,*], **Kun Di**[2], **Julien Bec**[2], and **Simon R. Cherry**[2]

[1]School of Engineering, University of California, Merced, California 95343, USA

[2]Department of Biomedical Engineering, University of California, Davis, California 95616, USA

Abstract

We present a hybrid imaging modality, x-ray luminescence optical tomography (XLOT), in which collimated x-ray beams are used to excite phosphor-based contrast agents. Images are reconstructed from the optical signals, using the known x-ray beam location and spatial extent as priors. We demonstrate XLOT using phantom experiments with deep targets and show that the reconstructed signal varies by <12% when the depth changes from 4.2 to 7.7 mm. For simple source distributions, we find as few as two orthogonal projection measurements are sufficient for XLOT reconstruction.

Hybrid imaging combines the strengths of two imaging modalities. Examples include photoacoustic tomography [1,2] and x-ray acoustic computed tomography [3], in which a pulsed laser or x-ray source, respectively, are used to generate ultrasound inside tissue. Another example is the emerging technique of x-ray luminescence computed tomography (XLCT) that combines the high sensitivity of optical detection with the high spatial resolution of x-ray imaging [4,5]. Here, we propose a related approach, x-ray luminescence optical tomography (XLOT), which utilizes a collimated x-ray beam to excite deep embedded targets together with optical propagation modeling, permitting reconstruction of the distribution of phosphor-particle-based contrast agents in turbid media overlaid on a structural CT image. This overcomes the ill-posedness of the inverse problem in fluorescence and bioluminescence optical tomography [6–8] and provides a pathway for high-resolution *in vivo* optical molecular imaging at significant depths inside tissue.

In XLOT, collimated x-ray beams are used to excite contrast agents that have been injected into the subject and are based on phosphor particles such as Eu^{3+}-doped gadolinium oxysulfide (GOS:Eu^{3+}). This phosphor has a high cross section for diagnostic energy x rays, excellent light yield, and the emitted light is primarily between 600 and 750 nm, which is good for tissue penetration (Fig. 1). Nanoscale x-ray excitable particles of GOS:Eu^{3+} and other Eu^{3+}-doped lanthanide compounds have been successfully synthesized [9–10]. These particles can be made biocompatible (e.g., using a gold shell) and ultimately functionalized for molecular imaging applications.

*Corresponding author: cli32@ucmerced.edu.

Figures 1 and 2(a) show the geometry for XLOT. A collimated x-ray beam is scanned across the sample. Optical photons emitted by GOS particles in the subject are detected with an electron-multiplying charge coupled device (EMCCD). Knowing the volume of the subject excited by the x-ray beam, and using this as prior information, EMCCD measurements are used to reconstruct images of luminescence intensity (proportional to particle concentration), using a model-based reconstruction method similar to fluorescence optical tomography [11]. XLOT retains the advantage of high sensitivity common to optical detection, but its spatial resolution is dependent primarily on the x-ray beam size and is independent of the target depth. The inverse problem also is far less ill posed, as light emission (except that caused by scattered x rays) is largely limited to the small volume excited by the x-ray beam at each measurement location. By detecting the transmitted beam with an x-ray detector, a structural x-ray CT image also can be reconstructed.

The following components and methods were used in our experimental system. The x-ray tube (SB80250, Oxford Instruments) was controlled with commercial software (Source-ray, Inc.) and generates x-ray photons up to a maximum energy of 80 kVp and tube current of 0.25 mA. The x-ray detector (Shado-box 1024, GOS scintillator screen, Rad-Icon Imaging Corporation) had a detection area of 49.2 mm by 49.2 mm consisting of a 1024 by 1024 element photodiode array sensor with 48 μm pixels. The x-ray beam was collimated using a 5.08 cm long, 2.54 cm diameter steel rod with a central 1 mm diameter hole. Phantoms were placed on a motorized rotation stage (B4872TS-ZR, Velmex, Inc.) mounted on a motorized linear stage (MB250901J-S3, Velmex, Inc.). The collimated x-ray beam scanned the phantoms using 32 linear steps for each projection angle with a step size of 1 mm. The emitted optical photons on the top surface were reflected with a mirror and imaged by an EMCCD camera (C9100-13, Hamamatsu). Bandpass filters were mounted inside the filter wheel to allow for selection of the detected photon wavelengths. The EMCCD was placed inside a 5 mm thick lead box that shields the EMCCD from high-energy x-ray photons. The whole system was placed in an x-ray- and light-shielded enclosure.

A cylindrical phantom (50 mm long, 32 mm diameter), composed of 1% intralipid and 2% agar, was used to mimic the volume and scattering properties of a mouse. An offset cylindrical target (4.8 mm diameter, 48 mm long), composed of 1% intralipid, 2% agar, and GOS:Eu^{3+} (UKL63/UF-R1, Phosphor Technology Ltd.) at different concentrations, was embedded in the cylinder. Figure 2(a) shows the phantom geometry—the embedded target is offset 7.5 mm radially and 2 mm below the top surface. The following three sets of phantom experiments were performed: (1) phantoms with GOS:Eu^{3+} target concentrations of 1 mg/ml were scanned with the x-ray beam at a depth of $H = 4.2$ mm. XLOT images were reconstructed from a single angular projection, two orthogonal projections, and 36 projections. Exposure time per projection element was 30 s for the one and two projection datasets and 5 s for the 36 projection dataset. (2) Using a target concentration of 10 mg/ml, data were taken for x-ray beam depths of $H = 4.2$, 5.9, and 7.7 mm. Two projections were used for reconstruction. Exposure time was 20 s per projection element. (3) Two targets each with a GOS:Eu^{3+} concentration of 10 mg/ml were embedded in the phantom, at radial offsets of 8.6 and 7.9 mm. The scanning depth was $H = 4.2$ mm. Exposure time was 15 s per projection element. Two projections were used for reconstruction. The radiation dose in

these experiments was estimated by Monte Carlo methods to be consistent with *in vivo* microCT studies.

For all measurements the EMCCD camera was operated at $-92°C$ and set at EMgain 255 and analog gain 5. The x-ray tube current was 0.24 mA at a tube voltage of 75 kVp. The x-ray detector exposure time was fixed at 450 ms. Images from the x-ray detector provided the x-ray pencil beam location and size and were used to reconstruct CT images. X-ray CT images were reconstructed from the pencil beam x-ray data using a standard filtered backprojection algorithm. For phantom set 1, the reconstructed CT image is shown in Fig. 2(b).

The XLOT reconstruction algorithm has been described in detail elsewhere [12]. Briefly, we model optical photon propagation with the diffusion equation solved with the finite element method. The preconjugated gradient (PCG) method is used to minimize the difference between measured and modeled photon intensity and to update XLOT images. The pencil beam x-ray dimensions and location are included in the reconstruction algorithm as priors. Figures 2(c)–2(e) show reconstructed XLOT images for GOS:Eu^{3+} concentrations of 1 mg/ml, using 1, 2, and 36 angular projections. The target is reconstructed successfully at the correct location. In this simple case, two projection measurements are sufficient to reconstruct XLOT images. With only one angular projection, artifacts are introduced [Fig. 2(c)]. The short exposure time for the 36-projection study resulted in increased noise in the reconstructed XLOT image [Fig. 2(e)]. At a GOS:Eu^{3+} concentration of 1 mg/ml, there is insufficient difference in x-ray attenuation to visualize the target using x rays [Fig. 2(b)]. Thus XLOT is a much more sensitive technique than x-ray CT in this particular situation. However, the CT image is still useful as a structural/anatomical reference image to define the location of XLOT signals.

Figure 3 shows reconstructed XLOT images for varying x-ray beam depths. The reconstructed maximum values in the target area vary by <12% between the three different depths, even though the raw detected signal changes by more than 50%. Figure 3(d) shows the reconstructed XLOT image for the phantom containing two embedded targets and for an x-ray beam depth of 4.2 mm. The two targets are resolved and reconstructed in the correct location.

This initial prototype system and methodology suffers from a number of limitations. Only the top surface of phantom was imaged using a simple flat mirror. For small-animal imaging applications, we propose a conical mirror geometry to collect photons from the whole surface of the body [11]. Limited by scanning time, only a single 2D cross section of the phantom was scanned and reconstructed, although XLOT can readily be extended to 3D. Optimized x-ray illumination patterns for reducing XLOT scanning time are being studied. X-ray attenuation is not currently modeled in the XLOT reconstruction algorithm, which is why the right target has slightly higher reconstructed values than the left target in Fig. 3(d). The measurements in this work used 2 μm GOS:Eu^{3+} particles. Nanoscale GOS:Eu^{3+} particles that will be needed for *in vivo* applications may have different emission efficiencies. We have not yet calibrated XLOT in order to absolutely quantify the phosphor concentration, nor determined the linear range, spatial resolution, or detection limits. The

ultimate performance of the method depends on many factors including x-ray tube settings and beam collimation, EMCCD quantum efficiency and noise levels, phosphor absorption/emission efficiencies, tissue optical properties and accurate modeling of x-ray attenuation, scatter, and light propagation. We are currently studying these factors and optimizing performance/settings where possible to develop a practical system suitable for *in vivo* imaging studies.

In summary, we developed a prototype XLOT imaging system to detect x-ray luminescent particles embedded in turbid media. We have experimentally demonstrated the feasibility of XLOT for sensitive imaging of deep targets with good spatial resolution. XLOT also provides a CT image as a structural reference. This hybrid approach offers significant promise for sensitive, high-resolution optical molecular imaging in small animals, using targeted nanoparticle probes based on phosphor cores.

Acknowledgments

This work was funded in part by R21 EB013828 from the National Institutes of Health.

References

1. Wang XD, Pang YJ, Ku G, Xie XY, Stoica G, Wang LHV. Nat. Biotechnol. 2003; 21:803. [PubMed: 12808463]
2. Razansky D, Vinegoni C, Ntziachristos V. Opt. Lett. 2007; 32:2891. [PubMed: 17909608]
3. Xiang L, Han B, Carpenter C, Pratx G, Kuang Y, Xing L. Med. Phys. 2013; 40:010701. [PubMed: 23298069]
4. Pratx G, Carpenter CM, Sun C, Rao RP, Xing L. Opt. Lett. 2010; 35:3345. [PubMed: 20967061]
5. Pratx G, Carpenter CM, Sun C, Xing L. IEEE Trans. Med. Imaging. 2010; 29:1992. [PubMed: 20615807]
6. Ntziachristos V, Ripoll J, Wang LHV, Weissleder R. Nat. Biotechnol. 2005; 23:313. [PubMed: 15765087]
7. Wang G, Cong WX, Durairaj K, Qian X, Shen H, Sinn P, Hoffman E, McLennan G, Henry M. Opt. Express. 2006; 14:7801. [PubMed: 19529149]
8. Schulz RB, Ale A, Sarantopoulos A, Freyer M, Soehngen E, Zientkowska M, Ntziachristos V. IEEE Trans. Med. Imaging. 2010; 29:465. [PubMed: 19906585]
9. Wang H, Wang R, Sun X, Yan R, Li Y. Mater. Res. Bull. 2005; 40:911.
10. Tian Y, Cao WH, Luo XX, Fu Y. J. Alloys Compd. 2007; 433:313.
11. Li C, Mitchell GS, Dutta J, Ahn S, Leahy RM, Cherry SR. Opt. Express. 2009; 17:7571. [PubMed: 19399136]
12. Li C, Martinez Davalos A, Cherry SR. Proc. SPIE. 2013; 8578:85781B.

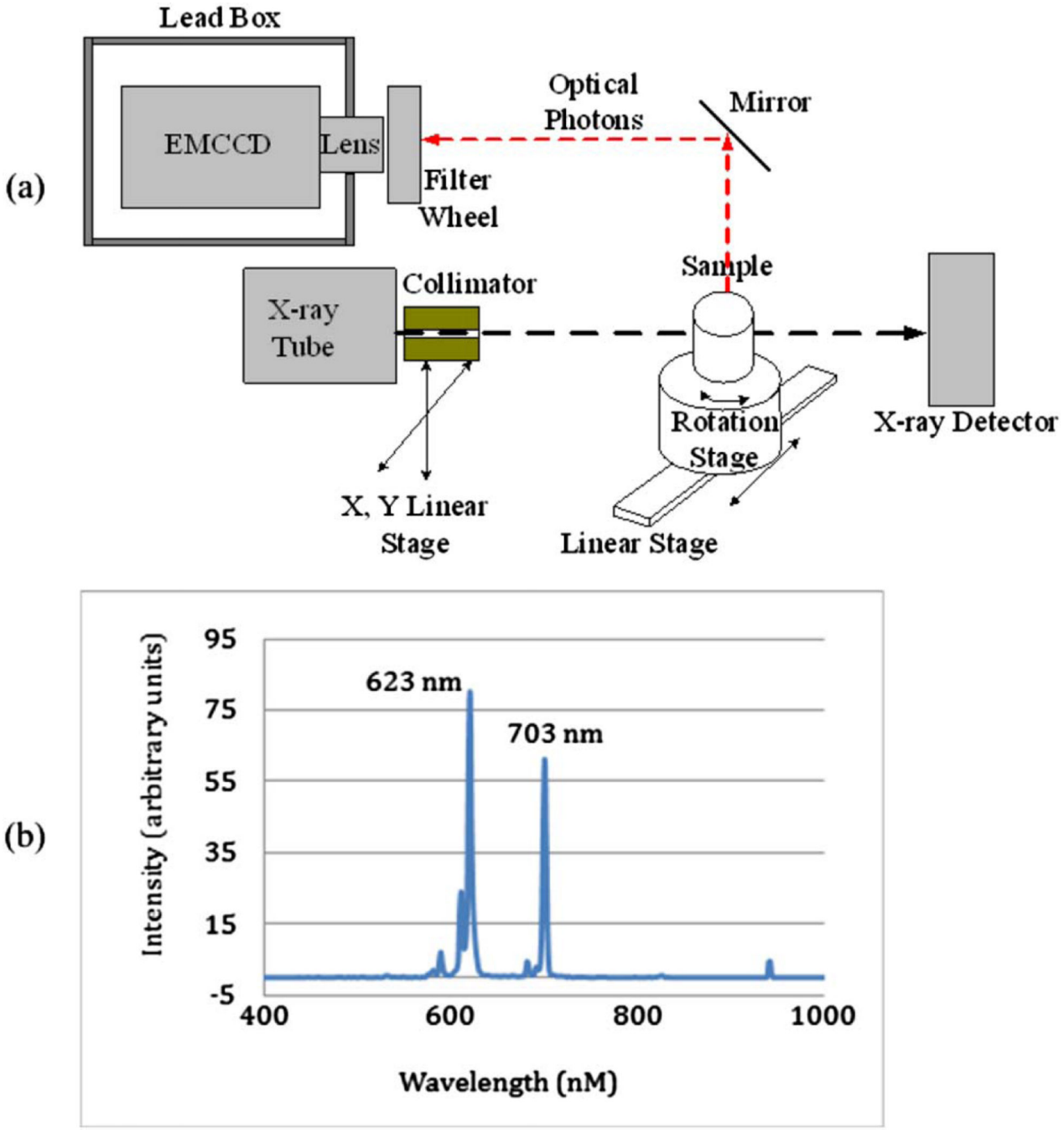

Fig. 1.

(a) Schematic of the prototype XLOT imaging system. (b) Emission spectrum of GOS:Eu powder following x-ray excitation.

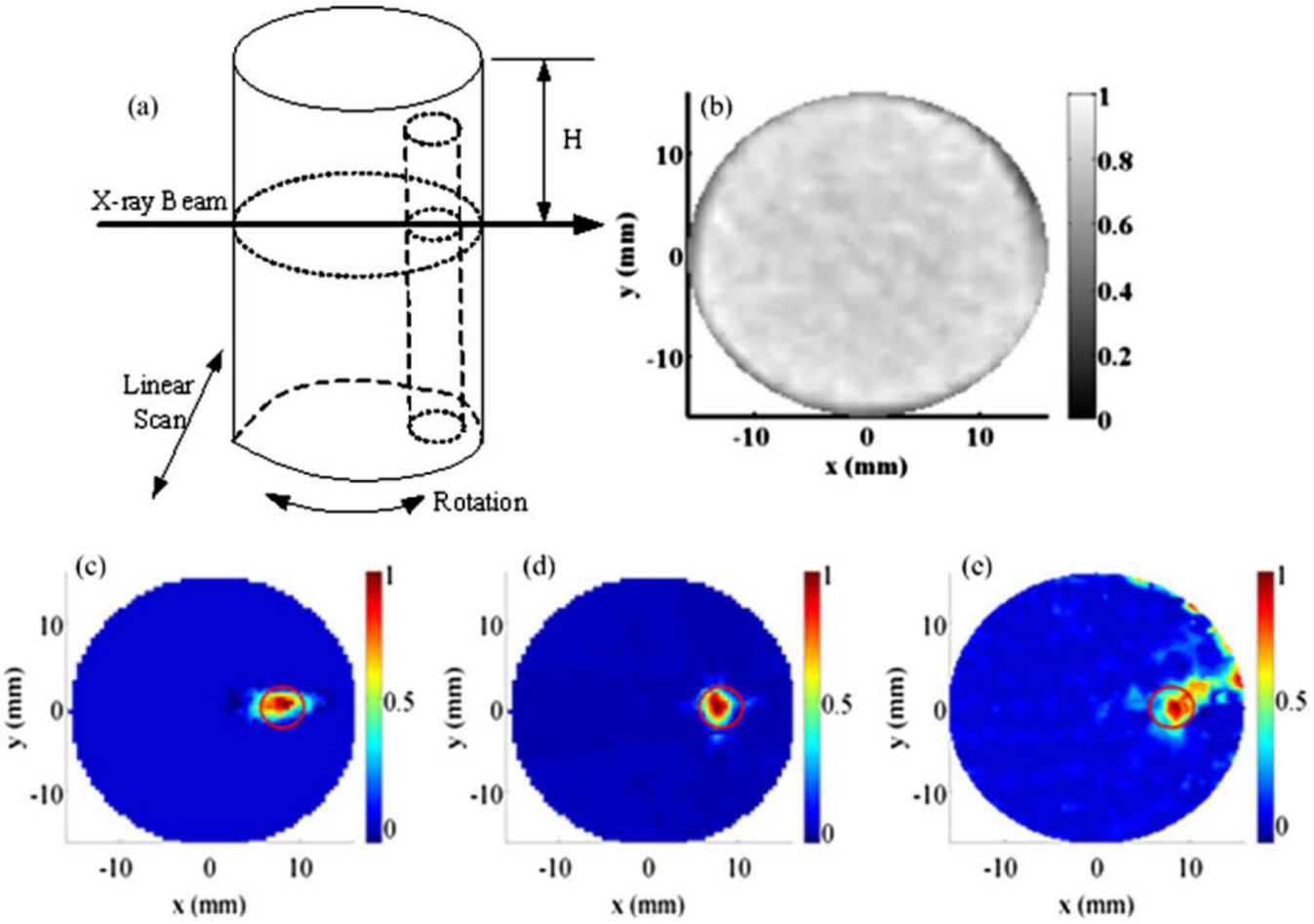

Fig. 2.

(a) Schematic of a phantom and the scanning scheme. (b) Reconstructed pencil beam CT image for phantom set 1. (c) Reconstructed XLOT images for GOS:Eu concentration of 1 mg/ml with 1 projection measurement, (d) 2 projection measurements, and (e) 36 projection measurements. The red circle indicates the actual target location.

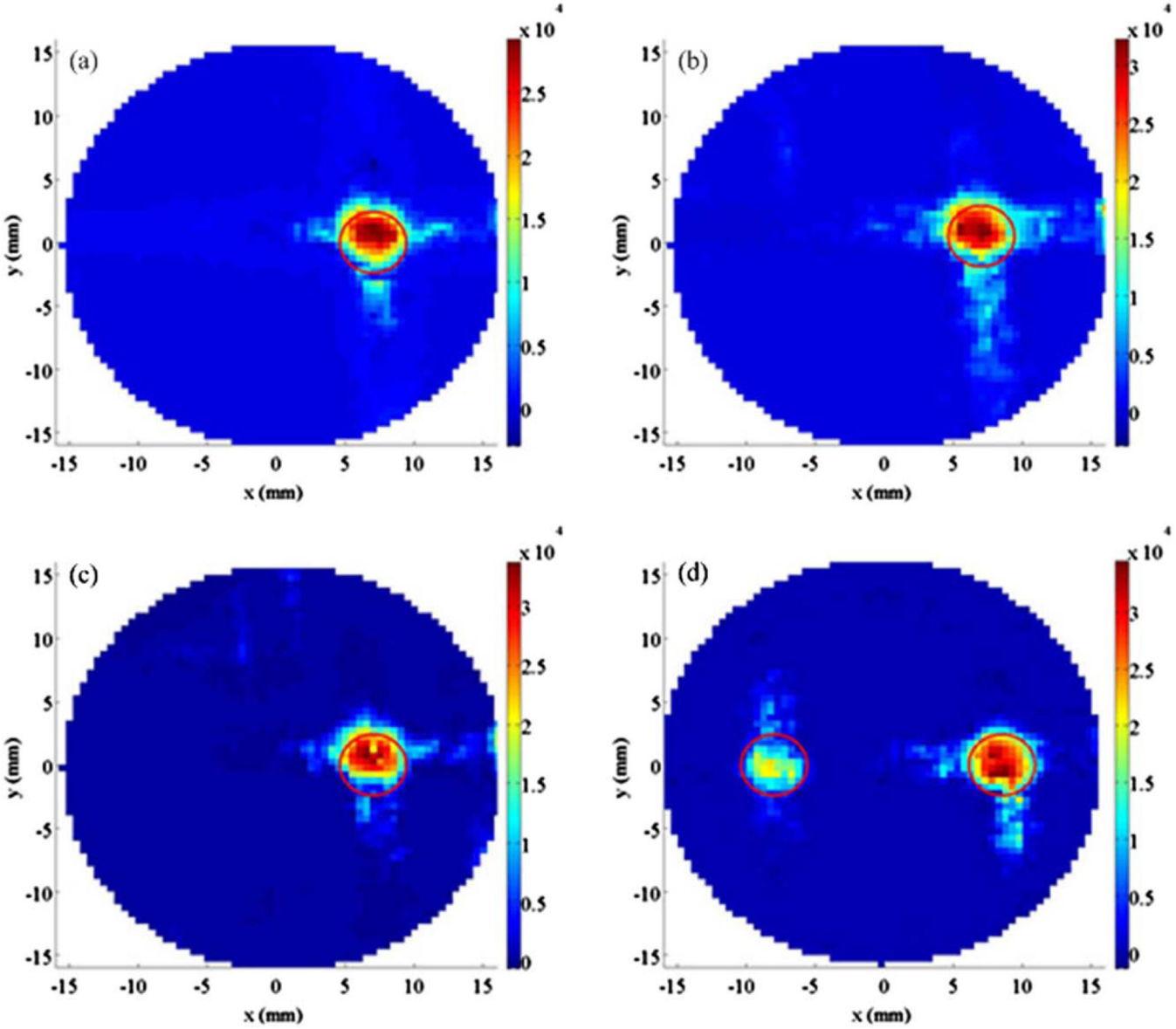

Fig. 3.

Reconstructed XLOT images at depths of (a) 4.2 mm, (b) 5.9 mm, and (c) 7.7 mm (phantom set 2). (d) For multiple target case (phantom set 3), reconstructed XLOT image at depth of 4.2 mm. Two projection measurements were used. The red circles indicate the known target location.